



Cite this: *RSC Adv.*, 2024, 14, 17824

Turn-on mode probe based on the sustainable xanthohumol extract for the efficient viscosity response in a liquid system†

Lingfeng Xu, *^{abc} Xinya Liu,^a Jingyi Zhao,^a Xinmin Deng^a and Hui Peng^a

Viscosity is a typical physical parameter and plays an important role in nutrient transferring, diffusion process regulating and safety warning. Aberrant mitochondrial viscosity is closely associated with an imbalance in a liquid system. Nevertheless, there is currently a lack of convenient and efficient tools for the mutation of viscosity detection at the molecular level. Herein, a natural product xanthohumol (XTH) was extracted from *Humulus lupulus* and used to measure the microenvironmental viscosity. Due to the existence of carbonyl and phenolic hydroxyl groups, a typical twisted intramolecular charge transfer (TICT) was formed. The conjugated single and double bonds can be employed as the rotatable site. Consequently, a turn-on method based on viscosity response is developed. High sensitivity ($x = 0.56$) with a remarkable enhancement (55-fold) toward viscosity and a visualized fluorescent signal can be found. In addition, it displays a single selectivity with excellent photostability and pH stability in the complex liquid system. Using the extracted XTH, a typical application toward the liquid spoilage process was performed and a positive correlation was noted. Given the comprehensive properties of XTH, liquid safety inspection at a molecular level with natural source-extracted products can be obtained.

Received 7th April 2024
Accepted 22nd May 2024

DOI: 10.1039/d4ra02612h
rsc.li/rsc-advances

Introduction

Viscosity is an important physical parameter in the microenvironmental liquid, which has great significance for the transduction, metabolism, and apoptosis processes.^{1,2} When liquid foods undergo deterioration and corruption, especially the growth of bacteria, the micro-environment in liquids is changed, leading to the stress response, homeostasis, and substance movement.^{3–5} Thus, the viscosity was changed. Previous studies have shown that the extent of deterioration is closely related to the viscosity of liquids.^{6,7} Importantly, the monitoring of the liquid micro-environment is of great significance to the warning and anticipating spoilage extent of liquids.⁸ Therefore, abnormal viscosity changes may be an acute physical indicator used to distinguish the normal ones from the deteriorated samples in a sensitive, green, and *in situ* pathway.

To date, several methods have been established for monitoring viscosity changes.^{9–12} Large volumes of samples and pre-processing time are required when using traditional

viscometers, and a limitation for micro-environmental viscosity detection still exists.^{13,14} Compared with these traditional methods, the fluorescent technique is more favored by researchers owing to its advantages of rapid response, simple operation, high sensitivity, and convenient process.^{15,16} The use of fluorescent probe not only greatly improves the efficiency but also can make it possible to transform the chemical and physical information into a detectable optical signal, *in situ* and at a molecular level.^{17,18} With the development of fluorescent materials and techniques, various conjugated probes have been designed, which strongly rely on the elaborate control process and tedious synthesis program.^{19,20} Many viscosity probes have been developed (as shown in Table S1, ESI†), which have been widely used in the biological fields such as tracking the mitochondrial viscosity,²¹ investigating the lysosomal viscosity,²² and sensing the physiological viscosity changes.^{23–26} It can be found that most of the reported probes contain the electron donor and acceptor and form a typical intramolecular charge transfer (ICT) system. The intramolecular rotation between electron donating group and electron withdrawing group in the molecules may lead to the twisted intramolecular transfer effect (TICT), weak or strong signal can be released with the status transferring.^{27,28} Thus far, relatively few probes from the naturally extracted product have been used to detect viscosity. Numerous organic solvents and complex synthesis procedures can be avoided. Thus far, several kinds of plant extracts have been applied in Chinese medicine, biological agents, oral liquids, *etc.*^{29,30}

^aKey Laboratory of Jiangxi Province for Special Optoelectronic Artificial Crystal Materials, Jinggangshan University, Ji'an, Jiangxi 343009, China

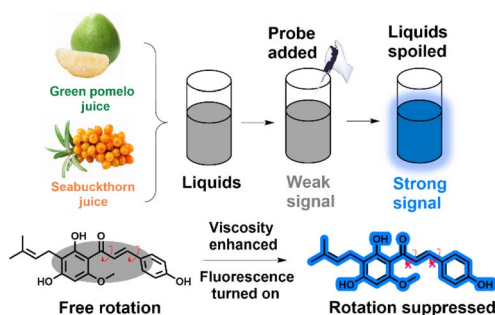
^bState Key Laboratory of Luminescent Materials & Devices, College of Materials Science & Engineering, South China University of Technology, Guangzhou 510640, China. E-mail: rs7jfxu@outlook.com

^cSchool of Chemistry and Chemical Engineering, Nanchang University, Nanchang, Jiangxi 330036, China

† Electronic supplementary information (ESI) available. See DOI: <https://doi.org/10.1039/d4ra02612h>


Natural products can offer unique functionalities, such as specific recognition capabilities, and self-assemble, into defined superstructures with unique shapes.³¹ Moreover, many researchers have found that these natural products can respond to multiple physical, chemical, and biological stimuli, and even display as a nano-medicine for disease intervention.^{32,33} Therefore, it is important to develop fluorescent probe with sustainable long-term evolution and natural, green, and eco-friendly features to trace viscosity in the liquid system.

Herein, based on the chemical structure finding, a natural product has been extracted from the hops and acts as the molecular probe named xanthohumol (**XTH**). As shown in Scheme 1, **XTH** is composed of conjugated single and double bonds as well as phenolic hydroxyl and carbonyl groups. Phenolic hydroxyl is the electron donor (D), and carbonyl acts together as the electron acceptor (A), which could form the typical D- π -A structure. We expected that the electron push-pull portion and free rotating C-C single bond could make the natural probe respond to viscosity based on the twisted intramolecular charge transfer (TICT). In the low-viscosity system, the single bond between the phenolic hydroxyl and carbonyl parts rotates freely, which causes the two parts not to be in the same plane and is accompanied by charge separation.^{34,35} In this status, **XTH** mainly occurs in a nonradiative transition, leading to energy loss, and the signal is weak.³⁶ Under a high-viscosity liquid system, the rotation is limited, which can inhibit TICT formation. Thus, the charge transfer recovers, which can result in enhanced fluorescence.^{37,38} The excited state of **XTH** conversion from the TICT state to the ICT state under different viscosity media can be applied to detect micro-environmental viscosity. The experimental results showed that the natural probe **XTH** exhibited a maximum emission peak around 425 nm, and a 'turn-on' mode was accompanied by a high coefficient ($x = 0.56$). In addition, **XTH** displays high specificity, sensitivity, and adaptability to viscosity, and real-time *in situ* tracking capability can be achieved. As a natural product, complex design and synthesis processes can be avoided, and low-carbon development goals can be practiced. The natural probe **XTH** can distinguish the abnormal viscosity during the spoilage process and provide a chance for interdisciplinary research using molecular tools.



Scheme 1 Viscosity sensing and spoilage detection mechanism of the activatable natural molecular probe **XTH**.

Experimental sections

Materials and methods

The chemical reagents in this study were directly obtained from Macklin Biotechnology (Shanghai) Co., Ltd, and Shanghai Aladdin Bio-Chem Technology Co., Ltd. All the reagents and solvents were used without any further purification. A Milli-Q water purification system (Millipore, Bedford, MA, USA) was used to prepare the deionized (DI) water. Nuclear magnetic resonance (NMR) spectra were obtained using a Bruker AVANCE III HD 400 NMR spectrometer, with TMS internal standard in DMSO- d_6 . High-resolution mass spectra (HR-MS) were performed using an Agilent 7250 and JEOL-JMS-T100LP AccuTOF mass spectrometer. Fluorescence spectra were recorded by applying a Hitachi F-7000 fluorescence spectrophotometer. Absorption spectra were detected using a Hitachi U-3010 UV-Vis spectrophotometer. The viscosity determination test was performed using a rotating viscometer (DV2T, Brookfield, AMETEK Corp., USA). The reagents and instruments were described in the ESI.[†]

Extraction of the xanthohumol (molecular probe **XTH**)

The hops (female flowers of *Humulus lupulus* L.) were sieved through a 1 mm sieve. The obtained sample was placed in a 50 mL screw-top vial fitted with a Teflon-lined screw cap in the choline chloride-based solvent. This mixture was stirred at 60 °C for 1 h in an oil bath. The resulting product was then cooled to room temperature, washed with DI water, and sieved with the extrusion press. After that, the washings were extruded with the choline chloride-based eutectic solvents (contained glycerol, ethylene glycol, propylene glycol, and lactic acid as a hydrogen bond donor) in a 100 mL conical centrifuge tube. With the addition of DI water, the mixture was incubated at a lower temperature (5 °C) for over 12 h and then separated by centrifugation for 8 min. This process was repeated 3 times, and methanol was added to the precipitate and vortexed for about 3 min. The supernatant after centrifugation was then transferred to the volumetric flask, and the methanol was added to the remaining precipitate, followed by vortexing for 1 min. The obtained solution (methanol extract) was transferred to a flask, and the solvent was removed. In the end, the products were purified with silica powder with column chromatography. ¹H NMR (400 MHz, DMSO- d_6) δ 12.04 (s, 1H), 10.12 (d, $J = 15.2$ Hz, 2H), 8.48 (d, $J = 14.7$ Hz, 1H), 8.18 (s, 1H), 7.95 (d, $J = 10.1$ Hz, 2H), 6.90 (d, $J = 9.3$ Hz, 2H), 6.45 (d, $J = 11.9$ Hz, 1H), 6.01 (d, $J = 9.5$ Hz, 1H), 3.92 (s, 1H), 3.22 (d, $J = 8.3$ Hz, 2H), 1.98 (t, $J = 4.7$ Hz, 3H), 1.75 (t, $J = 5.2$ Hz, 3H). ¹³C NMR (101 MHz, DMSO- d_6) δ 193.56, 152.32, 148.10, 147.46, 143.53, 133.20, 132.42, 129.39, 129.08, 127.71, 127.03, 124.79, 123.37. MS (ESI): m/z 355.15595 [$M + H$]⁺, calcd for $C_{21}H_{22}O_5$ 354.14672.

Optical properties investigation

The natural extract **XTH** was dissolved in the DMSO to prepare the stock solution with a concentration of 1.0 mM. During the optical test, **XTH** was diluted as 10 μ M, and the viscosity response was performed in the glycerol and DI water mixture.



The absorption spectra were taken in the common solvents, including the toluene, acetonitrile, *N,N*-dimethylformamide (DMF), dimethylsulfoxide (DMSO), methanol, ethyl acetate, glycerol and DI water. The solvent adaptability and the spectra properties of **XTH** were obtained, and each sample with six common solvents was utilized. The specificity of **XTH** was tested with various liquid additives and sodium salts (50 μM), such as Na^+ , K^+ , Cl^- , D-mannitol, acesulfame, and sorbitol. The natural probe **XTH** in each substance solution was controlled at 10 μM , and the detailed spectra properties were recorded. The effects of temperature on viscosity were tested in the three typical conditions of 37 $^{\circ}\text{C}$, 5 $^{\circ}\text{C}$, and 25 $^{\circ}\text{C}$. Three representative thickeners (from 1 g kg^{-1} to 5 g kg^{-1}) of xanthan gum (XG), pectin (Pec), and sodium carboxymethyl cellulose (SCC) were prepared as standard test solutions. Before the experiments, bubbles in the solutions were eliminated. The emission wavelength was set as 320 nm, and the corresponding data can be recorded in the range of 350–600 nm.

Viscosity checking process

We purchased two kinds of commercial fresh fruit juices: green pomelo and seabuckthorn juices. Before the experiments, flesh floats and sediments were removed, and 1.06 mg **XTH** was added into the corresponding pomelo and seabuckthorn juices, respectively. Afterwards, both real samples were stored under ambient temperature (25 $^{\circ}\text{C}$) and lower maintenance temperature (5 $^{\circ}\text{C}$); the spectrometer was utilized, and the corresponding excitation wavelength was set at 320 nm. The relationship between fluorescence signal intensity and viscosity value is established: $(F_n - F_0)/F_0 = (\eta_n - \eta_0)/\eta_0$, where F_n and F_0 denote fluorescence intensity at day n and day 0, respectively; η_n and η_0 denote viscosity values at day n and day 0, respectively.

Theoretical calculation of the natural probe XTH

Theoretical calculations were performed *via* the Gaussian 09 program with the B3LYP/6-31G(d) level of theory, and the angle was optimized to 0 $^{\circ}$ and 90 $^{\circ}$. The energy gap and oscillator strength f_{em} were also calculated.

Results and discussion

Molecular rotor design and selected strategy

In a large number of natural extracts, **XTH** exhibited an excellent conjugated chemical structure, and the fluorescence signal could be released under certain circumstances. However, natural products have been utilized to construct functional materials in the industry field³⁹ because their degradable, sustainable, reproducible features, and resources are considerable. A phenolic hydroxyl group (donor, D) and a carbonyl group (acceptor, A) exist in the chemical structure. The D and A groups were hosted in the **XTH** by coincidence, and a typical ICT structure was formed. A free rotation among the phenolic hydroxyl and carbonyl groups exists, and the signal can be switched among the off and on states when the excited dye senses the viscosity fluctuations in the thick and thin solutions. A non-radiative pathway can lead to the quenching of

fluorescence, and the relaxation pathway can lead to the releasing of fluorescence, which may be attributed to the state changing from the TICT to the ICT. Thus, the microenvironmental viscosity may be visualized. Consequently, the natural molecular probe is applied to monitor the commercial liquid safety, and the high-viscosity media (especially the spoiled ones) can be discriminated from the normal samples, as displayed in Scheme 1. Moreover, after the design strategy, the extract **XTH** was adequately characterized by ^1H NMR, ^{13}C NMR and HR-MS, as illustrated in Fig. S1–S3 (ESI[†]).

Optical properties toward viscosity

Based on the unique TICT structure of **XTH**, under the excitation of 320 nm wavelength light, the optical properties of **XTH** in typical viscous media (distilled water and glycerol) are investigated. As shown in Fig. 1a, the results showed that a higher fluorescence intensity can be observed in the glycerol, while a weak fluorescence intensity can be found in the distilled water. About 55-fold increment at 435 nm (maximum) was displayed. It was confirmed that the emission features in each viscous media can be visualized efficiently. In the meantime, the absorption spectra were also tested. As depicted in Fig. 1b, a slightly longer absorption wavelength (382.5 nm) and stronger fluorescence signal in the glycerol can be captured, while a shorter absorption wavelength (375.5 nm) and weaker fluorescence signal in the water were displayed. This is what distinguishes it from low-viscosity media and the higher-viscosity samples. The red-shifted phenomenon may be ascribed to the inhibited rotation and parallel stacking of molecules in the high-viscosity micro-environment. Moreover, the rising viscosity solution with a series of water–glycerol mixture systems under normal pH = 7.4 was investigated in

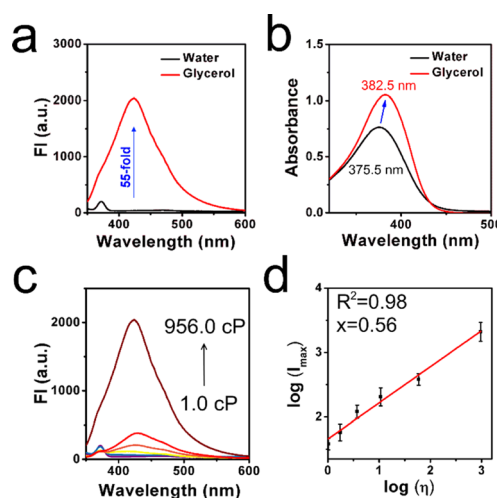


Fig. 1 (a) Absorption spectra of the molecular probe **XTH** in different solvents, such as water and glycerol. (b) Fluorescence spectra of the molecular probe **XTH** in different solvents, such as water and glycerol. (c) Fluorescence emissive spectra of the molecular probe **XTH** in different solvent systems, with the water–glycerol mixture with the fraction of glycerol (f_g) from 0% to 99%. (d) A linear relationship between $\log I_{\text{max}}$ and $\log \eta$.



detail (in Fig. 1c). A varied viscosity micro-environment (from 1.0 cP to 956.0 cP) was established, and a sharp gradual enhancement with the increased glycerol content (from 0% to 99%) was observed. An obvious turn-on mode was established. Quantitatively, the emission intensity $\log(I_{\max})$ was linearly fitted against the solution viscosity $\log(\eta)$ with a correlation coefficient of 0.98 by fitting the Förster–Hoffmann equation. As shown in Fig. 1d, the viscosity-sensitive coefficient was found to be $x = 0.56$.

The final intensity was approximately 53 times the initial intensity. In addition, the physical properties of quantum yields and fluorescence lifetime in water and glycerol are collected, as presented in Table S2 (ESI†). This result further confirmed its capability for viscosity sensing. Afterward, the Stokes shift in the water and glycerol were recorded from the absorption and emission spectra because a larger Stokes shift may be helpful to filter out the spontaneous signal. As depicted in Fig. S4a and b (ESI†), the results showed 91.7 nm in the low-viscosity water and 65.3 nm in the high-viscosity glycerol. This result is similar to most of the previous probes designed through the artificial synthesis trial (as displayed in Table S1, ESI†).

The emission properties of **XTH** were also studied under different temperatures (5 °C, 25 °C, and 37 °C) because viscosity is often changed by the temperature. In Fig. S5 (ESI†), the fluorescence intensity was compromised at 25 °C, while the signal was strongest at 5 °C and weakest at 37 °C. These findings indicate that the temperature has an obvious effect on the emission feature of **XTH**, and the fluctuation of viscosity caused by temperature can be recorded with the addition of **XTH**. Next, the detection limit of **XTH** was also performed, as shown in Fig. S6 (ESI†). The regression curve equation was obtained under a lower viscosity range, which was found to be 1.321 cP, ensuring the accuracy of viscosity testing.

During the commercial liquid juices, several kinds of food thickeners were added to enhance flavor and mellowness. Various viscosity micro-environments can be established with the addition of thickeners, and consistency, stability, and homogeneity of liquids can be enhanced as well. Thus, three kinds of representative thickeners were selected to observe the

fluorescence behavior of **XTH**, including the SCC, Pec, and XG. In Fig. 2a, the fluorescent intensities obviously enhanced with an increase from 1 g kg⁻¹ to 5 g kg⁻¹ due to the thickening effects. It can be found that the thickening efficiency of these thickeners was quite different; the determined highest thickening effect was XG, and the lowest thickening efficiency was SCC. The thickening process can be recorded using the fluorescent method with **XTH**. Quantitatively, the slope between the fluorescence intensity and thickener addition was established. In Fig. 2b, the slope in the SCC sample was 17.06, while the slope of the XG sample reached 106.73. A large slope was ascribed to the higher thickening efficiency, and the results are consistent with the emission tests. Moreover, the spectral response performance of the natural probe **XTH** in various commercial liquids was measured using the fluorescent technique. As shown in Fig. S7 (ESI†), ten kinds of commercial liquids were tested, and different emission intensities can be found. **XTH** displayed a weak fluorescence signal in the common fresh juices, and with the increase in viscosity, the fluorescence intensity was enhanced significantly in the edible oil and glycerol. Detailed data were collected, as presented in Table S3 (ESI†), and the differences of viscosity can be determined with the existence of natural probe **XTH**. The calculated viscosity values obtained from the fluorescent method were consistent with the data obtained from the traditional viscometer, as shown in Table S4 (ESI†). The results demonstrated that the rotation of the C=C double bond around the single bond in the **XTH** can be utilized as the sensing point. Therefore, the fluorescence intensity of **XTH** was enhanced with increased viscosity and decreased with lower viscosity. The capacity of **XTH** to accurately measure viscosity was confirmed, and the viscosity changes caused by the solution contents, temperatures, thickeners, and potential applications in various commercial liquids (especially in the lower viscosity media) could be captured with the natural probe **XTH**.

Photostability, selectivity, response mechanism and theoretical calculation

A photostability test of **XTH** was conducted, and the fluorescence response of **XTH** in different kinds of commercial liquids was investigated. As depicted in Fig. S8 (ESI†), the fluorescence intensity of **XTH** remains stable under continuous light irradiation for 60 min, which ensures stable signal output and accurate results during the detection process. The results indicated that **XTH** has high photostability and is suitable for practical applications even in complex commercial liquids. Subsequently, the effects of pH and storage duration on the fluorescence intensities of **XTH** in the broad pH solutions were evaluated (as illustrated in Fig. S9, ESI†). When the pH values were in the range of 3.0–7.4, the fluorescence intensities remained stable. When the pH values increased from 7.4 to 10.0, a slight increase occurred. However, little enhancement cannot affect the robust stability of pH changes. The results show that it possesses pH tolerance under wider physiological conditions. The effect of polarity in the liquid system is quite important, and based on the structural traits of natural probe

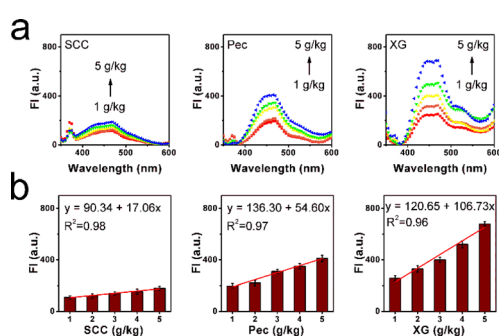


Fig. 2 (a) Emissive spectra of the molecular probe **XTH** in the thickening solvents in the presence of various mass amounts of sodium carboxymethyl cellulose (SCC), pectin (Pec) and xanthan gum (XG). (b) Emission intensity of the molecular probe **XTH** in the corresponding thickening media, and fitting line with the mass amounts of SCC, Pec, and XG.

XTH, we assumed that **XTH** had good spectroscopic stability toward the polarity. Herein, there are eight kinds of representative solvents, including water, DMF, toluene, acetonitrile, methanol, DMSO, ethyl acetate and glycerol. As shown in Fig. 3a, the absorption and emission spectra of these common solvents with different polarities were recorded. The absorption peaks were around 360 nm, and the absorbances were similar. Only a slight bathochromic shift phenomenon occurred in the high-viscosity glycerol. However, a more significant fluorescent signal was released in the glycerol than in the other solvents in the emission spectra. The emission signal cannot be affected by the polarity of solvents, and the natural probe **XTH** is suitable for use in complex liquid systems. Furthermore, adaptability in common solvents was investigated, and apparent fluorescent images were captured using the digital camera, as shown in Fig. 3b. The fluorescence signals in the common liquids were quite weak, whereas the signal released from glycerol was obviously stronger. These findings indicated that there was a turn-on mode toward viscosity detection, and a TICT effect appeared during the rotation process when it occurred in

viscous media. Detailed photo-physical properties in different solvents were collected, as shown in Table S5 (ESI†). Thus, **XTH** can discriminate viscosity changes from lower ones, and a higher signal-to-noise ratio can be found along with various polarities.

Commercial liquid has a complex microenvironment system, which includes active functional small molecules, additives, and inorganic salts. To observe the fluorescence behaviour of **XTH** to different analytes, solutions with various cations, anions, glucose, vitamin, and food additives were prepared. As illustrated in Fig. 3d, after the addition of the mentioned analytes (50 μ M) with the natural probe **XTH** solution (10 μ M), only high viscous glycerol induced the formation of a significant emission peak at 435 nm. Many representative species displayed weak signals. The emission histograms showed a fuller demonstration of the stability of the results, as shown in Fig. 3d. None of these analytes can cause viscosity changes, and only an obvious turn-on signal can be found in higher viscous media. This indicates that **XTH** still showed a relatively steady fluorescence intensity in the complex microenvironment, and the selectivity was high enough for viscosity detection.

To elucidate the response mechanism, the solvatochromism of **XTH** was measured. As shown in Fig. 4a and b, a slight bathochromic shift phenomenon occurred in the absorption and emission spectra, and an ICT effect existed between the hydroxyl group (donor) and carbonyl group (acceptor). It can be proposed that free rotation between the donor and acceptor in a low viscous liquid system could result in the TICT effect, which weakens the emission intensity. By contrast, the intra-molecular rotation was hindered, which hampered the TICT effect and increased the fluorescence intensity.⁴⁰ Additionally, a dual emission phenomenon usually occurs in a typical TICT system.⁴¹ As shown in Fig. 3c, an obvious dual emission phenomenon existed in the blue circle. Then, a density functional theory (DFT) theoretical calculation based on the Gaussian 09 package was performed. The optimized structures of **XTH** under 0° and 90° are illustrated in Fig. S10 (ESI†). In the **XTH** structure, the electron density on the highest occupied molecular orbital (HOMO) is concentrated on the hydroxyl group, while the lowest unoccupied molecular orbital (LUMO) is positioned at the carbonyl unit. The occurrence suggested that **XTH** underwent an ICT process, and there was an energy

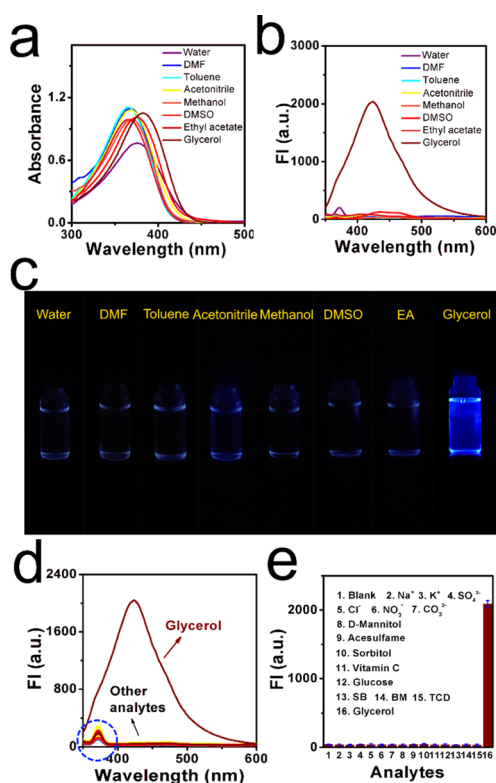


Fig. 3 (a) Absorption spectra of natural probe **XTH** (10 μ M) in eight kinds of representative solvents, including the water, DMF, toluene, acetonitrile, methanol, DMSO, ethyl acetate, and glycerol. (b) Emission spectra of natural probe **XTH** (10 μ M) in the representative solvents. (c) Emission images of natural probe **XTH** in different solvent systems. (d) Emission spectra of **XTH** (10 μ M) in various solutions with potential analytes in liquid food. (e) Histogram of the signal intensity of **XTH** with various analytes, including (1) blank, (2) Na^+ , (3) K^+ , (4) SO_4^{2-} , (5) Cl^- , (6) NO_3^- , (7) CO_3^{2-} , (8) D-mannitol , (9) acesulfame , (10) sorbitol , (11) vitamin C , (12) glucose , (13) $\text{sodium benzoate (SB)}$, (14) $\text{beet molasses (BM)}$, (15) $\text{trisodium citrate dehydrate (TCD)}$, and (16) glycerol .

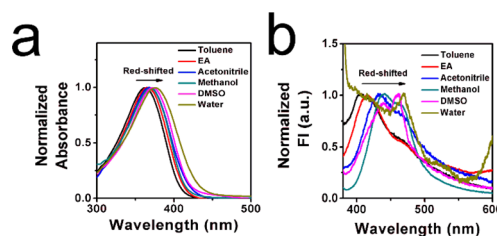


Fig. 4 (a) Normalized absorption spectra of **XTH** in toluene, EA, acetonitrile, methanol, DMSO, and water. (b) Normalized emissive spectra of molecular probe **XTH** in the six kinds of representative solvents.



transition process from the ground state to the excited state.⁴² Moreover, the energy gaps between hydroxyl (donor) and carbonyl (acceptor) can be calculated to be 3.7888 eV at dihedral angles of 0°, and 4.1146 eV at optimized 90°. When the phenolic hydroxyl group rotated by 0°, the f_{em} (oscillator strength) was also calculated as 0.1728, while when the phenolic hydroxyl group rotated by 90°, the f_{em} decreased to 0.0070. The results further suggested that the rotation was restricted, hampering the TICT effect and resulting in a poor emission signal. The theoretical calculations are consistent with the experimental results, which could confirm that **XTH** has a satisfactory response effect on viscosity.

Spoiled process tracking

As is well known, commercial juices usually contain a large number of nutrients, glucose, inorganic salts, *etc.* The viscosity can change with the deterioration process. We supposed that the viscosity-sensitive probe **XTH** could be applied to track this program at a molecular level. Thus, the green pomelo juice and seabuckthorn juice samples were stored under ambient temperature (25 °C) and lower maintenance temperature (5 °C), respectively. As shown in Fig. 5a, when these two kinds of liquid foods were stored under ambient temperature, the turbid and vague in the green pomelo juice and colour lightening and small drifts can be found gradually, especially after 3 days of storage. Within the next couple of days (especially after one week), a serious floating phenomenon occurred. On the contrary, when the liquid samples were stored at lower maintenance temperatures (Fig. 5b), a slightly turbid phenomenon and the colour of the sea buckthorn remained deep and limpid, even after day 7. From the digital images, it can be concluded

that a lower storage temperature can slow down the deterioration program and maintain freshness to some extent. With the help of **XTH**, the spoiled process can be tracked using the fluorescent method. As shown in Fig. 5c, the fluorescent intensity was recorded during the storage timeline on day 0, day 3, day 5, and day 7. When the juices were stored at ambient temperature, 18.2% and 17.1% enhancements were found. By contrast, when the samples were stored at lower maintenance temperatures, only 7.8% and 6.1% enhancements occurred after one week (Fig. 5d). From the naked eye, the emission fluorescence signal of green pomelo and seabuckthorn juices under different temperatures were investigated as well, as shown in Fig. S11 (ESI†). It can be observed that the fluorescence signal occurred at its highest when stored at room temperature, while negative enhancements can be found when stored at lower temperatures. The results were consistent with apparent images recorded by the digital camera, which indicates that **XTH** can distinguish the spoiled samples from normal ones *via* the fluorescent technique, and the fluctuation of viscosity during the spoilage process can be tracked quantitatively using the spectrometer.

However, viscosity values were determined using a viscometer. As depicted in Fig. 6a and b, the viscosity values of green pomelo and seabuckthorn juices increased by 21.8% and 20.7% when stored at 25 °C, respectively. However, under lower maintenance temperatures, 9.2% and 8.5% enhancements after one week were observed. We found that the viscosity values increased significantly after day 2, which means that the fresh juice spoiled more at ambient temperatures than at lower maintenance temperatures. The results obtained from the viscometer are consistent with the percentage-increased range

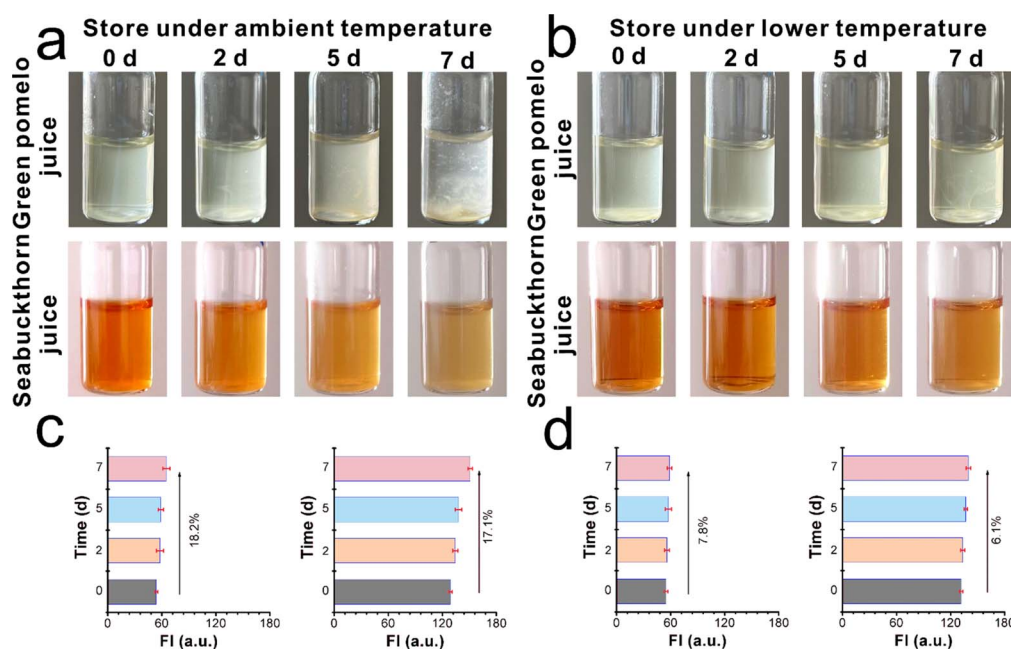


Fig. 5 Digital images of the green pomelo and seabuckthorn juices stored under (a) ambient temperature and (b) lower maintenance temperature within 7 days. The fluorescence signal intensity enhancements of green pomelo and seabuckthorn juices during the 7 days under (c) ambient temperature and (d) lower-maintenance temperature. The concentration of **XTH** = 10 μ M and λ_{ex} = 320 nm.



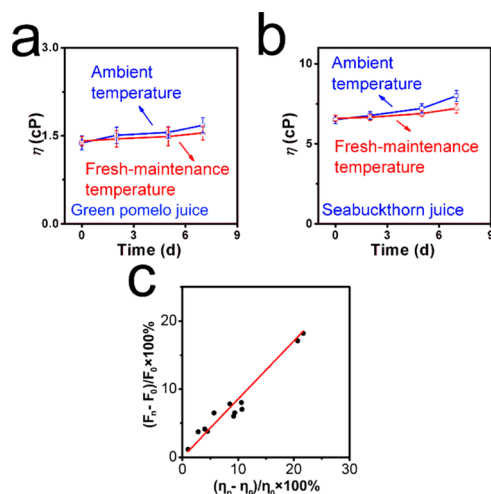


Fig. 6 (a) Viscosity values of green pomelo juice stored at different temperatures. (b) Viscosity values of seabuckthorn juice when stored at different temperatures. (c) Fitting line between the fluorescence increment percentage and viscosity-enhanced degree.

through the spectrometer. As illustrated in Fig. 6c, a fitting line between the fluorescence intensity enhancements $(F_n - F_0)/F_0 \times 100\%$ and the viscosity changes $(\eta_n - \eta_0)/\eta_0 \times 100\%$ is established. Both test results indicate that the natural probe **XTH** can be employed as a molecular tool to visualize micro-environmental viscosity changes during the deterioration process.

Conclusions

In summary, we have successfully extracted one kind of natural product named xanthohumol (**XTH**) as a molecular tool. With rotatable single- and double-conjugated bonds in the chemical structure, a TICT-based natural probe was developed to accurately distinguish and sensitively monitor dynamic changes in viscosity. An obvious turn-on signal can be observed with the enhancement (53-fold at maximum) of micro-environmental viscosity. The optical test results showed that the **XTH** had higher sensitivity ($x = 0.56$), good photostability, wider adaptability, and stronger selectivity. This suggests that **XTH** provides a reliable method for the detection of multiple factors at the molecular level and is a potential tool for application in complex commercial liquids. In addition, this natural probe **XTH** has a good pH and polarity tolerance. Importantly, this study verified that the **XTH** had the potential for micro-environmental viscosity tracking during the liquid spoilage process, which could provide a visualized means to accurately distinguish the spoiled samples from the normal ones. A linear relationship can be established between the fluorescence signal intensities and viscosity values using the fluorescent and traditional viscometer methods. This study not only testified that **XTH** could be a powerful tool to image viscosity in a sustainable green and low-carbon pathway but also could provide a powerful and promising method for broad application in various interdisciplinary research fields.

Author contributions

Lingfeng Xu: conceptualization, writing – original draft, methodology, funding acquisition. Xinya Liu & Jingyi Zhao: formal analysis, investigation. Xinmin Deng: validation, visualization, software. Hui Peng: resources, writing – review & editing.

Conflicts of interest

There are no conflicts to declare.

Acknowledgements

This study was supported by the Natural Science Foundation of Jiangxi Province (20232BAB204029), Ji'an City Science and Technology Plan Project Public Safety 1 ([2023]18, 2022-201751), Research Fund of Jinggangshan University (JZ2301), Doctoral Research Foundation of Jinggangshan University (JZB2006), Innovation and Entrepreneurship Training Program for College Students of Jinggangshan University (JDX2023126), Innovation and Entrepreneurship Training Program for College Students of Jiangxi Province (S202310419039).

References

- 1 J. Yin, L. Huang, L. Wu, J. Li, T. D. James and W. Lin, *Chem. Soc. Rev.*, 2021, **50**, 12098–12150.
- 2 H. Li, H. Kim, C. Zhang, S. Zeng, Q. Chen, L. Jia, J. Wang, X. Peng and J. Yoon, *Coord. Chem. Rev.*, 2022, **473**, 214818.
- 3 S. Feng, S. Gong, Z. Zheng and G. Feng, *Sens. Actuators, B*, 2022, **351**, 130940.
- 4 X. Yang, X. Lu, J. Wang, Z. Zhang, X. Du, J. Zhang and J. Wang, *J. Agric. Food Chem.*, 2022, **70**, 3047–3055.
- 5 Z. Wang, Y. Zhang, Y. Liang, M. Li, Z. Meng, Y. Yang, X. Xu and S. Wang, *J. Agric. Food Chem.*, 2022, **70**, 669–679.
- 6 M. Ma, Q.-J. Sun, M. Li and K.-X. Zhu, *Food Chem.*, 2020, **318**, 126495.
- 7 Z. Liang, Y. Sun, R. Duan, R. Yang, L. Qu, K. Zhang and Z. Li, *Anal. Chem.*, 2021, **93**, 12434–12440.
- 8 X. Zhang, F. Huo, Y. Zhang, Y. Yue and C. Yin, *Analyst*, 2022, **147**, 2470–2476.
- 9 J. Nsor-Atindana, H. D. Goff, W. Liu, M. Chen and F. Zhong, *Carbohydr. Polym.*, 2018, **200**, 436–445.
- 10 E. Lee, B. Kim and S. Choi, *Sens. Actuators, A*, 2020, **313**, 112176.
- 11 N. Mäkelä, O. Brinck and T. Sontag-Strohm, *Food Hydrocolloids*, 2020, **100**, 105422.
- 12 W.-N. Wu, Y.-F. Song, X.-L. Zhao, Y. Wang, Y.-C. Fan, Z.-H. Xu and T. D. James, *Chem. Eng. J.*, 2023, **464**, 142553.
- 13 J. Yin, X. Kong and W. Lin, *Anal. Chem.*, 2021, **93**, 2072–2081.
- 14 Y. Jia, Z. Cheng, G. Wang, S. Shuang, Y. Zhou, C. Dong and F. Du, *Food Chem.*, 2023, **402**, 134245.
- 15 C. Gao, Q. Huang, Q. Lan, Y. Feng, F. Tang, M. P. M. Hoi, J. Zhang, S. M. Y. Lee and R. Wang, *Nat. Commun.*, 2018, **9**, 2967.
- 16 S.-L. Xu, F.-F. Guo, Z.-H. Xu, Y. Wang and T. D. James, *Sens. Actuators, B*, 2023, **383**, 133510.



- 17 X. Zhi, B. Shen and Y. Qian, *New J. Chem.*, 2020, **44**, 8823–8832.
- 18 W. Liu, T. Wang, L. Wang, Y. Wang, S. Hu and D. Tian, *Spectrochim. Acta, Part A*, 2024, **304**, 123329.
- 19 J.-T. Hou, K.-K. Yu, K. Sunwoo, W. Y. Kim, S. Koo, J. Wang, W. X. Ren, S. Wang, X.-Q. Yu and J. S. Kim, *Chem*, 2020, **6**, 832–866.
- 20 Y. Tang, Y. Ma, J. Yin and W. Lin, *Chem. Soc. Rev.*, 2019, **48**, 4036–4048.
- 21 S. Li, P. Wang, W. Feng, Y. Xiang, K. Dou and Z. Liu, *Chem. Commun.*, 2020, **56**, 1050–1053.
- 22 J. Cui, H. Nie, S. Zang, S. Su, M. Gao, J. Jing and X. Zhang, *Sens. Actuators, B*, 2021, **331**, 129432.
- 23 X. Zhang, H. Yan, F. Huo, J. Chao and C. Yin, *Sens. Actuators, B*, 2021, **344**, 130244.
- 24 L. Lian, R. Zhang, S. Guo, Z. Le, L. Dai, Y. Ren, X. Yu, J. Hou and J. Shen, *Chin. Chem. Lett.*, 2023, **34**, 108516.
- 25 L. Hu, D. Shi, X. Li, J. Zhu, F. Mao, X. Li, C. Xia, B. Jiang, Y. Guo and J. Li, *Dyes Pigm.*, 2020, **177**, 108320.
- 26 H. Li, W. Shi, X. Li, Y. Hu, Y. Fang and H. Ma, *J. Am. Chem. Soc.*, 2019, **141**, 18301–18307.
- 27 J. Wu, W. Liu, J. Ge, H. Zhang and P. Wang, *Chem. Soc. Rev.*, 2011, **40**, 3483–3495.
- 28 L. Fan, Y. Pan, W. Li, Y. Xu, Y. Duan, R. Li, Y. Lv, H. Chen and Z. Yuan, *Anal. Chim. Acta*, 2021, **1149**, 338203.
- 29 A. A. Elkordy, R. R. Haj-Ahmad, A. S. Awaad and R. M. Zaki, *J. Drug Delivery Sci. Technol.*, 2021, **63**, 102459.
- 30 C. Yao, J. Zhang, J. Li, W. Wei, S. Wu and D. Guo, *Nat. Prod. Rep.*, 2021, **38**, 1618–1633.
- 31 A. Kumar and V. Kumar, *Chem. Rev.*, 2014, **114**, 7044–7078.
- 32 K. Cung, B. J. Han, T. D. Nguyen, S. Mao, Y.-W. Yeh, S. Xu, R. R. Naik, G. Poirier, N. Yao, P. K. Purohit and M. C. McAlpine, *Nano Lett.*, 2013, **13**, 6197–6202.
- 33 W. Gao, X. Feng, A. Pei, C. R. Kane, R. Tam, C. Hennessy and J. Wang, *Nano Lett.*, 2014, **14**, 305–310.
- 34 R. Miao, J. Li, C. Wang, X. Jiang, Y. Gao, X. Liu, D. Wang, X. Li, X. Liu and Y. Fang, *Adv. Sci.*, 2022, **9**, 2104609.
- 35 T. Debnath and H. N. Ghosh, *ChemistrySelect*, 2020, **5**, 9461–9476.
- 36 Y. Liang, Y. Zhao, C. Lai, X. Zou and W. Lin, *J. Mater. Chem. B*, 2021, **9**, 8067–8073.
- 37 Y.-L. Zheng, X.-C. Li, W. Tang, L. Xie, F. Dai and B. Zhou, *Sens. Actuators, B*, 2022, **368**, 132169.
- 38 M. Sun, T. Wang, X. Yang, H. Yu, S. Wang and D. Huang, *Talanta*, 2021, **225**, 121996.
- 39 R. Mohammadinejad, S. Karimi, S. Iravani and R. S. Varma, *Green Chem.*, 2016, **18**, 20–52.
- 40 H. Su, J. Wang, X. Yue, B. Wang and X. Song, *Spectrochim. Acta, Part A*, 2022, **274**, 121096.
- 41 X. Feng, Y. Chen, Y. Lei, Y. Zhou, W. Gao, M. Liu, X. Huang and H. Wu, *Chem. Commun.*, 2020, **56**, 13638–13641.
- 42 L. Fan, X. Wang, Q. Zan, L. Fan, F. Li, Y. Yang, C. Zhang, S. Shuang and C. Dong, *Anal. Chem.*, 2021, **93**, 8019–8026.

